

Coherent spin-exchange via a quantum mediator

Timothy Alexander Baart^{1†}, Takafumi Fujita^{1†}, Christian Reichl², Werner Wegscheider²
and Lieven Mark Koenraad Vandersypen^{1*}

Coherent interactions at a distance provide a powerful tool for quantum simulation and computation. The most common approach to realize an effective long-distance coupling ‘on-chip’ is to use a quantum mediator, as has been demonstrated for superconducting qubits^{1,2} and trapped ions³. For quantum dot arrays, which combine a high degree of tunability⁴ with extremely long coherence times⁵, the experimental demonstration of the time evolution of coherent spin–spin coupling via an intermediary system remains an important outstanding goal^{6–25}. Here, we use a linear triple-quantum-dot array to demonstrate a coherent time evolution of two interacting distant spins via a quantum mediator. The two outer dots are occupied with a single electron spin each, and the spins experience a superexchange interaction through the empty middle dot, which acts as mediator. Using single-shot spin readout²⁶, we measure the coherent time evolution of the spin states on the outer dots and observe a characteristic dependence of the exchange frequency as a function of the detuning between the middle and outer dots. This approach may provide a new route for scaling up spin qubit circuits using quantum dots, and aid in the simulation of materials and molecules with non-nearest-neighbour couplings such as MnO (ref. 27), high-temperature superconductors²⁸ and DNA²⁹. The same superexchange concept can also be applied in cold atom experiments³⁰.

Nanofabricated quantum dot circuits provide an excellent platform for performing both quantum computation and simulation using single spins^{4,31,32}. Many approaches to implementing coherent spin coupling between distant quantum dots have been proposed, using a variety of coupling mechanisms. These include superconducting resonators^{6–8}, surface-acoustic wave resonators⁹, floating metallic¹⁰ or ferromagnetic couplers¹¹, collective modes of spin chains¹², superconductors^{13,14}, Klein tunnelling through the valence or conduction band¹⁵ and superexchange or sequential operations via intermediate quantum dots^{17–21}. A common theme among many of these proposals is to create a coupling between distant spins by virtual occupation of a mediator quantum system. So far, the use of these schemes to show the coherent time evolution of interacting distant spins is lacking. More broadly, there have been no experimental realizations, so far, of direct quantum gates between any type of solid-state spins at a distance.

In this Letter we focus on the superexchange interaction to induce spin–spin coupling at a distance. Superexchange is the (usually) antiferromagnetic coupling between two next-to-nearest-neighbour spins through virtual occupation of a non-magnetic intermediate state²⁷. Given that superexchange involves a fourth-order process in the hopping amplitude, it is challenging to use it to achieve coherent coupling. This is also the case for several related schemes relying on quantum mediators.

We use a linear triple-quantum-dot array with one electron on each of the outer dots and induce a superexchange interaction through the empty middle dot, which acts as a quantum mediator.

This induces spin exchange of the two distant electron spins. Using repeated single-shot spin measurements we record the coherent time evolution of the spin states on the outer dots. We control the superexchange amplitude via detuning of the middle dot electrochemical potential relative to those of the outer dots and study the crossover between superexchange and conventional nearest-neighbour spin exchange.

The dot array is formed electrostatically in a two-dimensional electron gas (2DEG) 85 nm below the surface of a GaAs/AlGaAs heterostructure (Fig. 1a, quantum dots shown as three dotted circles). Gate electrodes fabricated on the surface (see Methods) are biased with appropriate voltages to selectively deplete regions of the 2DEG and define the linear array of three quantum dots. The left and right dot are each occupied with one electron, and each of the two electrons constitutes a single spin-1/2 particle. The interdot tunnel couplings are set to ~8.5 GHz (left–middle) and ~11.8 GHz (middle–right). The sensing dot (SD, large dotted circle) next to the quantum dot array is used for non-invasive charge sensing using radiofrequency (RF) reflectometry to monitor the number of electrons in each dot³³. An in-plane magnetic field $B_{\text{ext}} = 3.2$ T is applied to split the spin-up (\uparrow) and spin-down (\downarrow) states of each electron by the Zeeman energy ($E_Z \approx 80$ μeV), defining a qubit. The electron temperature of the right reservoir is ~75 mK.

In this system, superexchange can be seen as the result of the effective tunnel coupling t_{SE} between the outer dots. The amplitude of superexchange, J_{SE} , is approximated by $-(t_{\text{SE}}^2/\epsilon)$, where ϵ is the detuning between the electrochemical potentials of the outer dots³¹ and $\epsilon = 0$ when (1,0,1) and (2,0,0) are degenerate. Here t_{SE} can be described as $t_{\text{SE}} = (t_{m,l} t_{m,r})/\delta$, where $t_{m,l}$ ($t_{m,r}$) is the tunnel coupling between the middle and left (right) site and δ is the detuning between the electrochemical potential of (1,1,0) and the average of the electrochemical potentials of (1,0,1) and (2,0,0)³⁴. The superexchange amplitude can thus be approximated as

$$J_{\text{SE}} = -\frac{t_{m,l}^2 t_{m,r}^2}{\delta^2 \epsilon} \quad (1)$$

(Supplementary Section V shows the range of validity), which illustrates the characteristic fourth-order hopping process underlying superexchange.

To provide direct evidence of coherent superexchange, we will probe the resulting time evolution of the two spins via repeated single-shot measurements using spin-to-charge conversion²⁶. To achieve high readout fidelities, we work at large magnetic field and perform the spin-to-charge conversion as close as possible to the charge sensor (SD). In previous work, we shuttled electrons consecutively from left to middle to right, with no detectable sign of spin flips upon shutting³⁵. Here, we explore a different approach, transferring the spin from left to right with only virtual occupation of the middle dot, using the same long-range tunnel coupling that underlies coherent superexchange²⁵. We test the two-spin readout

¹QuTech and Kavli Institute of Nanoscience, TU Delft, 2600 GA Delft, The Netherlands. ²Solid State Physics Laboratory, ETH Zürich, 8093 Zürich, Switzerland.

*These authors contributed equally to this work. *e-mail: l.m.k.vandersypen@tudelft.nl

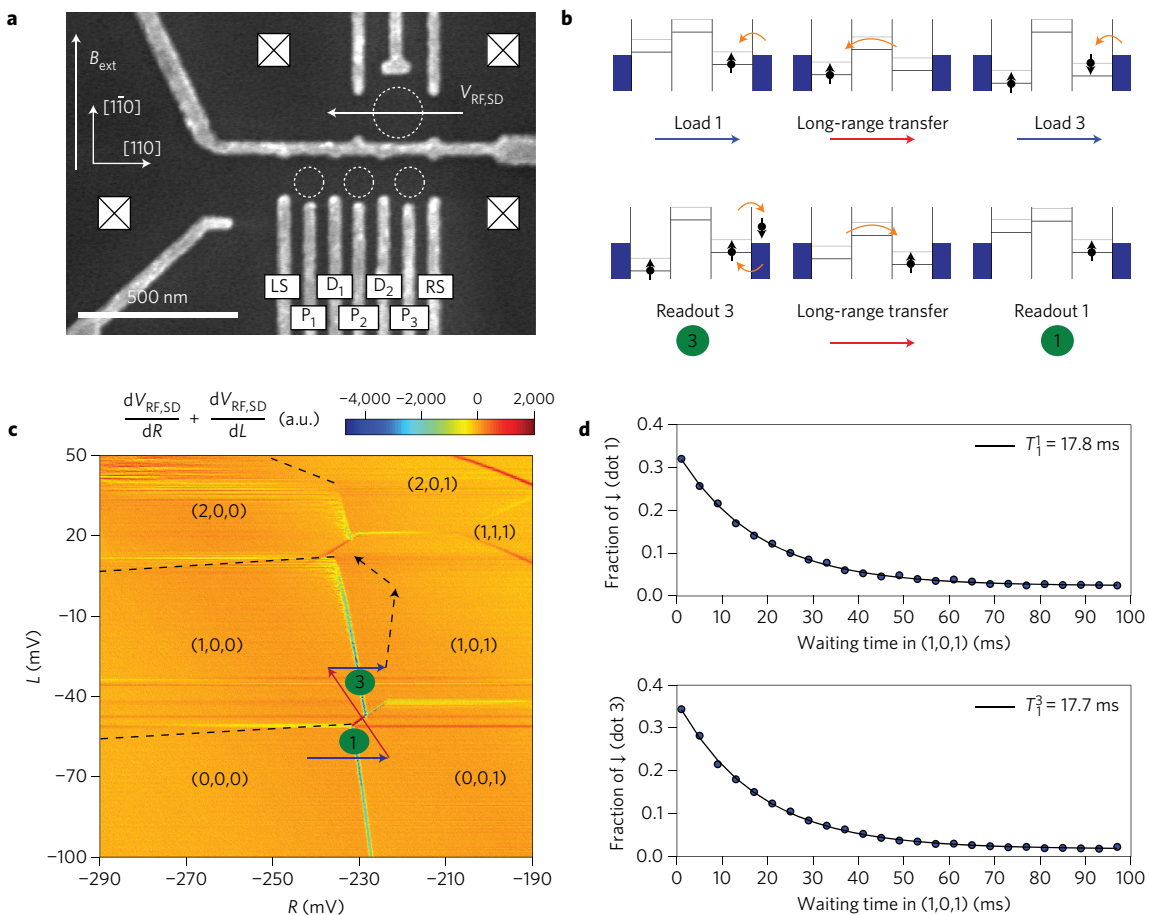


Figure 1 | Linear array of three quantum dots and long-range spin transfer. **a**, Scanning electron microscopy image of a sample nominally identical to the one used for the measurements. Dotted circles indicate quantum dots and squares indicate Fermi reservoirs in the 2DEG, which are connected to ohmic contacts. The RF reflectance of the SD is monitored to determine the occupancies of the three dots (labelled 1 to 3 from left to right). **b**, Read from left to right and top to bottom. The array is initialized by loading two electrons from the right reservoir. The spin that is loaded first is transferred to the left dot via a second-order tunnel process across the middle dot. We load \uparrow -spins by tuning the loading position such that only the \uparrow -spin level is accessible (as in the top left diagram). Random spins are loaded by making both spin levels energetically available (top right). Spin readout occurs using energy-selective tunnelling combined with charge detection via the SD. Labels (n,m,p) indicate the number of electrons in the left, middle and right dot, respectively. The middle dot cannot be loaded directly from a reservoir and the left dot is only weakly tunnel-coupled to the left reservoir, leading to faintly visible charge transitions (black dashed lines indicate their positions). The pulse sequence for loading and readout is indicated in the charge stability diagrams by blue and red arrows (also in b). The two black dashed arrows denote additional stages to probe superexchange (Fig. 2). **c**, Charge stability diagram of the triple dot for $M = -412$ mV. Along the L and R axes, we linearly vary the voltages applied to gates P_1 , P_2 and P_3 in such a way that we affect mostly the left and right dots, compensating for cross-capacitances. Similarly, M mostly controls the middle dot (Supplementary Section II). Labels (n,m,p) indicate the number of electrons in the left, middle and right dot, respectively. The middle dot cannot be loaded directly from a reservoir and the left dot is only weakly tunnel-coupled to the left reservoir, leading to faintly visible charge transitions (black dashed lines indicate their positions). The pulse sequence for loading and readout is indicated in the charge stability diagrams by blue and red arrows (also in b). The two black dashed arrows denote additional stages to probe superexchange (Fig. 2). **d**, Measured single-spin populations averaged over 8,000 cycles per data point as a function of waiting time in $(1,0,1)$ for dot 1 (top) and dot 3 (bottom).

and long-range spin transfer as described by the schematic diagrams in Fig. 1b and implemented by the pulse sequence depicted by the blue and red arrows in Fig. 1c. Starting from an empty array, we load a random electron from the reservoir into the right dot by pulsing into the charge state $(0,0,1)$. Next we pulse into $(1,0,0)$, whereby the electron is transferred from the rightmost dot to the leftmost dot via a second-order tunnel process across the middle dot. For this transfer we temporarily pulse δ closer to 0 to increase the long-range shuttling rate (Supplementary Section I). Finally, we once more load a random electron into the right dot by pulsing to $(1,0,1)$. We vary the waiting time in $(1,0,1)$, during which spins relax to the spin ground state $|\uparrow\downarrow\uparrow\rangle$. We then reverse the pulse sequence and add two calibrated readout stages (denoted by green circles in Fig. 1b,c) where spin-to-charge conversion takes place. Figure 1d shows the measured decays to the ground-state spin-up for each of the two spins. We report readout fidelities of 95.9 and 98.0%, on average, for spin-down and spin-up respectively, assuming no spin flips during the spin transfer³⁵ (Supplementary Section III).

A key signature of superexchange-driven spin oscillations is their dependence on the detuning of the intermediate level (δ) (see equation (1)). We therefore created linear combinations of the gates P_1 , P_2 and P_3 in such a way that we can independently vary δ and ϵ , as can be seen in Fig. 2b. Superexchange occurs in the $(1,0,1)$ charge configuration, and the superexchange amplitude J_{SE} increases for less negative ϵ , which translates to an operating point closer to the $(2,0,0)$ configuration (Fig. 2a). Similarly, J_{SE} increases with less negative δ , up to the point where we cross the $(1,0,1)-(1,1,0)$ transition indicated by the black dashed line in Fig. 2b, and spin exchange between nearest-neighbour dots will dominate (Fig. 2c). To capture the expected time evolution, we must take into account a difference in Zeeman energies between the two dots, $\Delta E_Z = E_{Z,3} - E_{Z,1}$, arising from slight differences in the g-factor for each dot³⁵. Spin exchange defines one rotation axis, and the Zeeman energy difference an orthogonal axis, as shown in the Bloch sphere in Fig. 2d. In the experiment, ΔE_Z is fixed and J_{SE} can be controlled by gate voltage pulses, as already

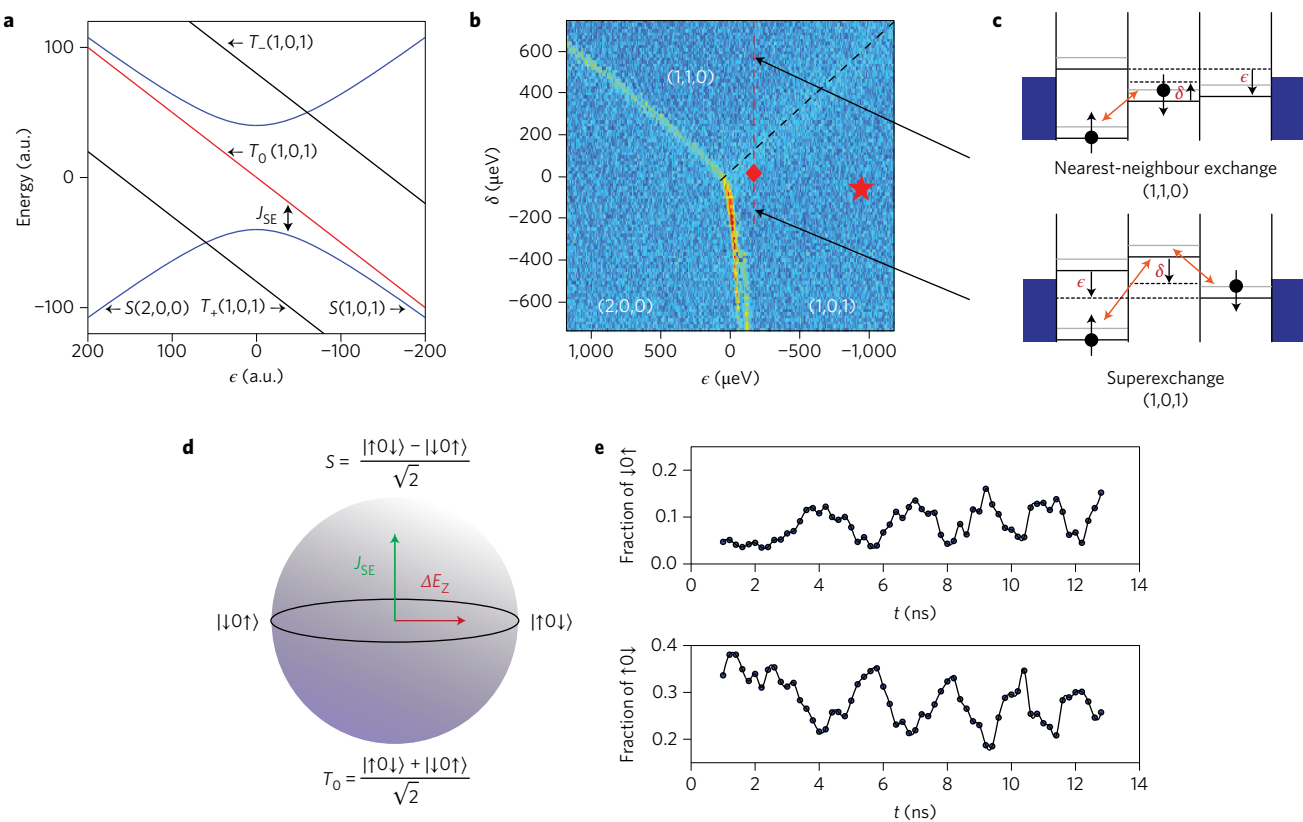


Figure 2 | Superexchange-driven spin oscillations. **a**, Energy diagram as a function of ϵ for $\delta < 0$. The long-range tunnel coupling induces an anti-crossing between the $(1,0,1)$ and $(2,0,0)$ singlet states. The energy difference between T_0 and the hybridized S is denoted J_{SE} . The T_- and T_+ states are split off by B_{ext} . **b**, Charge stability diagram in detuning space, allowing individual control of the detuning of the middle dot (δ) and between the outer dots (ϵ) (see **c**). **c**, Cartoon depicting the transition from superexchange to nearest-neighbour exchange as δ is made more positive. **d**, Bloch sphere representation of $S-T_0$ subspace in the superexchange regime with control axes J_{SE} and ΔE_Z . **e**, Observation of superexchange-driven spin oscillations. Starting with a mixture of $|↑0↓\rangle$ and $|↓0↑\rangle$ at the position of the red star in **b**, we pulse ϵ for a varying amount of time to the position indicated by the red diamond. Afterwards, the four two-spin probabilities are measured by averaging over 999 single-shot cycles per data point, two of which are shown.

discussed. By adjusting J_{SE} , we can thus define the net rotation axis and rate³⁶. A similar Bloch sphere can be made for the nearest-neighbour regime.

The protocol for probing the time evolution is as follows. Starting with an empty array, we create a mixture of $|↑0↓\rangle$ and $|↓0↑\rangle$ and move to the position of the red star in Fig. 2b, where J_{SE} is small compared to ΔE_Z . This is achieved by sequentially loading the two spins as in Fig. 1c, in this case loading a \uparrow in the left dot and a random spin in the right dot. This procedure allows us to conveniently create an antiparallel spin state without using more involved techniques such as electron spin resonance. Next, following the black dashed arrows in Fig. 1c, we pulse towards the $(2,0,0)$ regime and wait for several nanoseconds. The exact location in detuning space is marked in Fig. 2b by a red diamond. At this point J_{SE} is sizable, and $|↑0↓\rangle$ is not an eigenstate of the Hamiltonian and is thus expected to evolve in time, periodically developing a $|↓0↑\rangle$ component ($|↓0↑\rangle$ will only acquire an overall phase). The larger $J_{SE}/\Delta E_Z$, the larger the $|↓0↑\rangle$ component. We pulse back to the position of the red star in $(1,0,1)$ and follow the same spin readout procedure as was done for the T_1 measurement in Fig. 1d. Figure 2e shows the $|↑0↓\rangle$ and $|↓0↑\rangle$ probability as a function of the length of the detuning pulse. We see a sinusoidal dependence, with the $|↑0↓\rangle$ and $|↓0↑\rangle$ populations evolving in antiphase, as expected.

Returning to the key signature of superexchange, we fix the value of ϵ and vary δ along the vertical dashed red line shown in Fig. 2b. For each choice of δ , we record the four two-spin probabilities as a function of the length of the detuning pulse (Fig. 3a). Starting from

large negative δ , we first observe no oscillations at all: the superexchange mechanism is suppressed and the $|↑0↓\rangle$ state remains fixed along the x axis of the Bloch sphere. As the electrochemical potential of the intermediate level is brought closer to that of the outer dots, J_{SE} increases in magnitude, and slow oscillations of ~ 150 MHz start appearing that are still dominated by $\Delta E_Z \approx 130$ MHz between the outer dots, hence the low contrast of the oscillations. The oscillations become faster up to ~ 900 MHz as δ is increased, at which point J_{SE} is stronger than ΔE_Z and the contrast increases. When δ is further increased, the $(1,1,0)$ state becomes energetically favourable and the nearest-neighbour exchange between the left and middle dots dominates. Here $\epsilon = -170$ μeV and this transition occurs around $\delta = 120$ μeV, which is where the black dashed line in Fig. 2b is crossed. Increasing δ even more enlarges the detuning between the left and middle dots and thereby slows down the nearest-neighbour oscillations, as seen in the data.

For a quantitative comparison with theoretical predictions, we show in Fig. 3b the expected time evolution of the system modelled using the measured nearest-neighbour tunnel couplings, detunings δ and ϵ , and the difference in Zeeman energy probed through electric-dipole spin resonance measurements³⁷. We include the effect of dephasing by charge noise³⁶ to match the decay of the oscillations and account for the known readout fidelities and hyperfine-induced dephasing⁴ (Supplementary Section IV). We do not expect hyperfine-mediated electron spin flips in the present operating regime and hence no dynamical nuclear polarization. Figure 2e shows that it takes more than 1 ns for the superexchange to be turned on. This is caused by the finite rise time of the pulses

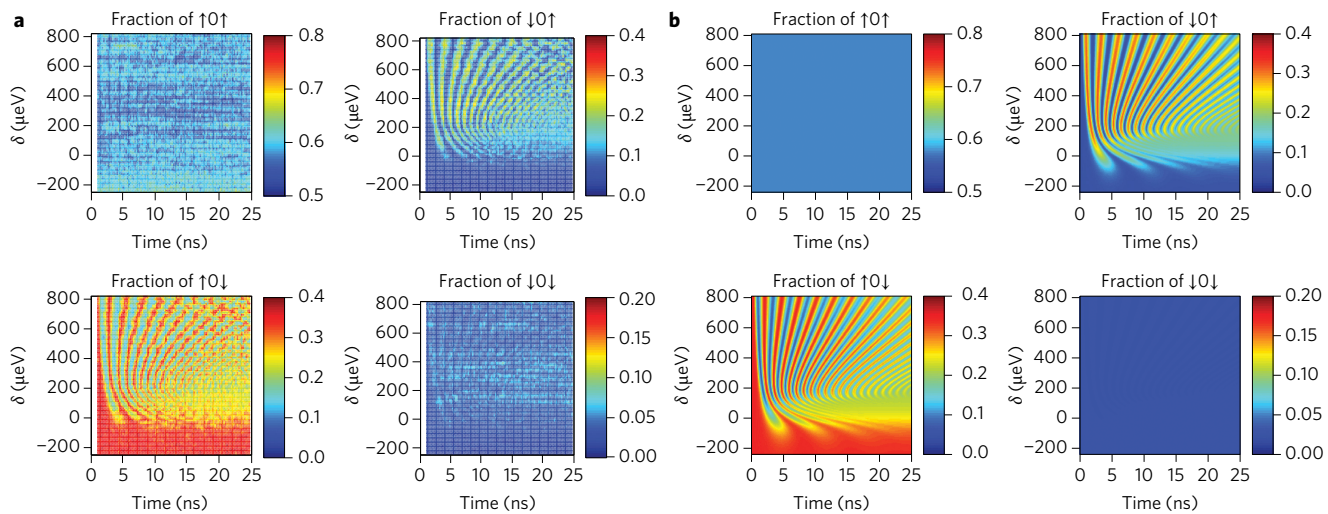


Figure 3 | Transition from superexchange to nearest-neighbour exchange. **a**, Starting with a mixture of $|\uparrow 0\downarrow\rangle$ and $|\uparrow 0\uparrow\rangle$ at the position of the red star in Fig. 2b, we pulse ϵ and δ for a varying amount of time to the position indicated by the vertical red dashed line in Fig. 2b. Afterwards, the four two-spin probabilities are measured by averaging over 999 single-shot cycles per data point. We clearly note the transition of oscillations dominated by ΔE_Z ($\delta < -50 \mu\text{eV}$) to increasingly faster superexchange-dominated spin evolution and finally ($\delta > 200 \sim \mu\text{eV}$) nearest-neighbour exchange-dominated evolution, which slows down as δ is further increased. Acquiring this set of data took ~ 20 h. **b**, Simulation of the data shown in **a**. The independently determined input parameters are $t_{m,l} = 8.5 \text{ GHz}$, $t_{m,r} = 11.8 \text{ GHz}$, $E_{Z,1} = 19.380 \text{ GHz}$, $E_{Z,2} = 19.528 \text{ GHz}$ and $E_{Z,3} = 19.510 \text{ GHz}$, and the rise time of the detuning pulse is 0.8 ns (Supplementary Section IV).

produced by the arbitrary waveform generator and finite bandwidth of the coax lines. The simulation includes this gradual turn on and off of J_{SE} . Comparing Fig. 3a,b, we report good agreement between theory and experiment, which supports our interpretation of the data in terms of superexchange, including the transition to nearest-neighbour exchange.

In summary, we have demonstrated a first working example of a direct quantum gate between solid-state spins at a distance via virtual occupation of a quantum mediator. This result underlines the utility of arrays of quantum dots for the investigation and application of fundamental physical processes driven by small-amplitude terms and higher-order tunnelling. It is possible to extend the distance between the coupled spins using elongated intermediate quantum dots or via different (quantum) mediators altogether. Another interesting direction is to create non-nearest-neighbour spin–spin interactions with the centre dot occupied^{20,21,24}, which opens up further new possibilities for quantum computation and modelling of complex materials.

Received 24 March 2016; accepted 24 August 2016;
published online 10 October 2016

References

- Majer, J. *et al.* Coupling superconducting qubits via a cavity bus. *Nature* **449**, 443–447 (2007).
- Sillanpää, M. A., Park, J. I. & Simmonds, R. W. Coherent quantum state storage and transfer between two phase qubits via a resonant cavity. *Nature* **449**, 438–442 (2007).
- Schmidt-Kaler, F. *et al.* Realization of the Cirac-Zoller controlled-NOT quantum gate. *Nature* **422**, 408–411 (2003).
- Hanson, R., Kouwenhoven, L. P., Petta, J. R., Tarucha, S. & Vandersypen, L. M. K. Spins in few-electron quantum dots. *Rev. Mod. Phys.* **79**, 1217–1265 (2007).
- Veldhorst, M. *et al.* A two-qubit logic gate in silicon. *Nature* **526**, 410–414 (2015).
- Taylor, J. M. & Lukin, M. D. Cavity quantum electrodynamics with semiconductor double-dot molecules on a chip. Preprint at <http://arxiv.org/abs/cond-mat/0605144v1> (2006).
- Burkard, G. & Imamoglu, A. Ultra-long-distance interaction between spin qubits. *Phys. Rev. B* **74**, 041307 (2006).
- Hu, X., Liu, Y. X. & Nori, F. Strong coupling of a spin qubit to a superconducting stripline cavity. *Phys. Rev. B* **86**, 035314 (2012).
- Schuetz, M. J. A. *et al.* Universal quantum transducers based on surface acoustic waves. *Phys. Rev. X* **5**, 031031 (2015).
- Trifunovic, L. *et al.* Long-distance spin–spin coupling via floating gates. *Phys. Rev. X* **2**, 011006 (2012).
- Trifunovic, L., Pedrocchi, F. L. & Loss, D. Long-distance entanglement of spin qubits via ferromagnet. *Phys. Rev. X* **3**, 041023 (2013).
- Friesen, M., Biswas, A., Hu, X. & Lidar, D. Efficient multiqubit entanglement via a spin bus. *Phys. Rev. Lett.* **98**, 230503 (2007).
- Leijnse, M. & Flensberg, K. Coupling spin qubits via superconductors. *Phys. Rev. Lett.* **111**, 060501 (2013).
- Hassler, F., Catelani, G. & Bluhm, H. Exchange-interaction of two spin qubits mediated by a superconductor. *Phys. Rev. B* **92**, 235401 (2015).
- Trauzettel, B., Bulaev, D. V., Loss, D. & Burkard, G. Spin qubits in graphene quantum dots. *Nat. Phys.* **3**, 192–196 (2007).
- Frey, T. *et al.* Dipole coupling of a double quantum dot to a microwave resonator. *Phys. Rev. Lett.* **108**, 046807 (2012).
- Mehl, S., Bluhm, H. & DiVincenzo, D. P. Two-qubit couplings of singlet–triplet qubits mediated by one quantum state. *Phys. Rev. B* **90**, 045404 (2014).
- Lehmann, J., Gaita-Arino, A., Coronado, E. & Loss, D. Spin qubits with electrically gated polyoxometalate molecules. *Nat. Nanotech.* **2**, 312–317 (2007).
- Sánchez, R., Gallego-Marcos, F. & Platero, G. Superexchange blockade in triple quantum dots. *Phys. Rev. B* **89**, 161402 (2014).
- Stano, P., Klinovaja, J., Braakman, F. R., Vandersypen, L. M. K. & Loss, D. Fast long-distance control of spin qubits by photon-assisted cotunneling. *Phys. Rev. B* **92**, 075302 (2015).
- Srinivasa, V., Xu, H. & Taylor, J. M. Tunable spin–qubit coupling mediated by a multielectron quantum dot. *Phys. Rev. Lett.* **114**, 226803 (2015).
- Viennot, J. J., Dartiailh, M. C., Cottet, A. & Kontos, T. Coherent coupling of a single spin to microwave cavity photons. *Science* **349**, 408–411 (2015).
- Petersson, K. D. *et al.* Circuit quantum electrodynamics with a spin qubit. *Nature* **490**, 380–383 (2012).
- Busl, M. *et al.* Bipolar spin blockade and coherent state superpositions in a triple quantum dot. *Nat. Nanotech.* **8**, 261–265 (2013).
- Sánchez, R. *et al.* Long-range spin transfer in triple quantum dots. *Phys. Rev. Lett.* **112**, 176803 (2014).
- Elzerman, J. M. *et al.* Single-shot read-out of an individual electron spin in a quantum dot. *Nature* **430**, 431–435 (2004).
- Kramers, H. L’interaction entre les atomes magnétogènes dans un cristal paramagnétique. *Physica* **1**, 182–192 (1934).
- Kim, C. *et al.* Systematics of the photoemission spectral function of cuprates: insulators and hole- and electron-doped superconductors. *Phys. Rev. Lett.* **80**, 4245 (1998).
- Giese, B., Amaudrut, J., Köhler, A. K., Spormann, M. & Wessely, S. Direct observation of hole transfer through DNA by hopping between adenine bases and by tunnelling. *Nature* **412**, 318–320 (2001).
- Meinert, F. *et al.* Quantum gases. Observation of many-body dynamics in long-range tunneling after a quantum quench. *Science* **344**, 1259–1262 (2014).
- Loss, D. & DiVincenzo, D. P. Quantum computation with quantum dots. *Phys. Rev. A* **57**, 120 (1998).

32. Barthelemy, P. & Vandersypen, L. M. K. Quantum dot systems: a versatile platform for quantum simulations. *Ann. Phys.* **525**, 808–826 (2013).
33. Barthel, C. *et al.* Fast sensing of double-dot charge arrangement and spin state with a radio-frequency sensor quantum dot. *Phys. Rev. B* **81**, 161308 (2010).
34. Braakman, F. R., Barthelemy, P., Reichl, C., Wegscheider, W. & Vandersypen, L. M. K. Long-distance coherent coupling in a quantum dot array. *Nat. Nanotech.* **8**, 432–437 (2013).
35. Baart, T. A. *et al.* Single-spin CCD. *Nat. Nanotech.* **11**, 330–334 (2016).
36. Dial, O. E. *et al.* Charge noise spectroscopy using coherent exchange oscillations in a singlet–triplet qubit. *Phys. Rev. Lett.* **110**, 146804 (2013).
37. Shafiei, M., Nowack, K., Reichl, C., Wegscheider, W. & Vandersypen, L. Resolving spin-orbit- and hyperfine-mediated electric dipole spin resonance in a quantum dot. *Phys. Rev. Lett.* **110**, 107601 (2013).

Acknowledgements

The authors acknowledge discussions with the members of the Delft spin qubit team and sample fabrication by F.R. Braakman. The authors thank M. Ammerlaan, J. Haanstra, R. Roeleveld, M. Tiggelman and R. Vermeulen for technical support. The authors

acknowledge financial support from the Intelligence Advanced Research Projects Activity (IARPA) Multi-Qubit Coherent Operations (MQCO) Program, the Netherlands Organization of Scientific Research (NWO) Graduate Program, the Japan Society for the Promotion of Science (JSPS) Postdoctoral Fellowship for Research Abroad and the Swiss National Science Foundation.

Author contributions

T.A.B. and T.F. executed the experiment and analysed the data. C.R. and W.W. provided the heterostructure. T.A.B., T.F. and L.M.K.V. contributed to the interpretation of the data, and T.A.B. and L.M.K.V. wrote the paper, with comments from T.F.

Additional information

Supplementary information is available in the [online version of the paper](#). Reprints and permissions information is available online at [www.nature.com/reprints](#). Correspondence and requests for materials should be addressed to L.M.K.V.

Competing financial interests

The authors declare no competing financial interests.